International Journal of Nanomedicine

Dovepress
Taylor & Francis Group

Open Access Full Text Article

ORIGINAL RESEARCH

Therapeutic Potential of Injectable Supramolecular Hydrogels With Neural Stem Cell Exosomes and Active Ingredient Methylcellulose for Post-Stroke Neurological Recovery

Qiankun Zhang[1], Yupeng Wang[2], Zhihan Zhu[1], Waqas Ahmed[1,3], Dongfang Zhou[2], Lukui Chen[1]

[1]Department of Neurosurgery, Southern Medical University Hospital of Integrated Traditional Chinese and Western Medicine, Southern Medical University, Guangzhou, People's Republic of China; [2]Key Laboratory of Mental Health of the Ministry of Education, School of Pharmaceutical Sciences, Southern Medical University, Guangzhou, People's Republic of China; [3]School of Medicine, Southeast University, Nanjing, People's Republic of China

Correspondence: Lukui Chen, Department of Neurosurgery, Southern Medical University Hospital of Integrated Traditional Chinese and Western Medicine, Southern Medical University, Guangzhou, 510310, People's Republic of China, Email neuro_clk@hotmail.com; Dongfang Zhou, Key Laboratory of Mental Health of the Ministry of Education, School of Pharmaceutical Sciences, Southern Medical University, Guangzhou, People's Republic of China, Email dfzhou@smu.edu.cn

Background: Stroke has significantly contributed to the global mortality rate over the years, emphasizing the urgency of finding effective treatment strategies. Neural stem cell (NSC)-derived exosomes have the potential to improve neurological recovery after stroke; however, their therapeutic efficacy is hindered by their rapid clearance and limited duration of action. This study presents an innovative drug delivery method: a hydrogel based on NSC exosomes and active ingredient methylcellulose (HPMC), which is intended to offer a continuous release, thereby enhancing and prolonging neurological improvement.

Results: We developed a nanohydrogel (Exo-HPMC) by integrating Buyang Huanwu Decoction (BHD) -preconditioned NSC-derived exosomes with HPMC. This study thoroughly investigated the controlled-release capabilities and rheological properties of Exo-HPMC. Our findings show that Exo-HPMC enables effective sustained exosome release, significantly extending their retention in mice. When administered to mice with middle cerebral artery occlusion (MCAO), Exo-HPMC facilitated notable post-stroke neurorepair. Behavioral assessments and immunofluorescence staining demonstrated that exosomes significantly promoted angiogenesis and nerve regeneration in stroke-affected areas, thereby reversing programmed cell death.

Conclusion: The Exo-HPMC nanohydrogel presents a groundbreaking approach for stroke therapy. Ensuring a controlled and prolonged release of NSC-derived exosomes over two weeks, significantly enhances the therapeutic potential of exosomes for ischemic stroke treatment.

Keywords: stem cell, exosome, hydrogel, angiogenesis, neuroregeneration

Introduction

Stroke remains the second most common cause of adult mortality and is associated with substantial disability and a reduced quality of life. Ischemic stroke accounts for 85% of all cases.[1,2] The current clinical consensus for treatment includes mechanical thrombectomy and intravenous thrombolysis; however, their application is limited by a narrow therapeutic window.[3] Consequently, there is an increasing need for novel and effective treatments to improve patient outcomes. Early recirculation of the blood flow in the ischemic penumbra is crucial for promoting neurological recovery. Emerging research has highlighted the complex temporal and spatial dynamics of brain neurogenesis and angiogenesis.[4] Therefore, early recanalization of peri-infarct core blood flow is a therapeutic priority in stroke management.

Exosomes, nano-sized vesicles measuring 30–200 nm, have attracted considerable attention for their potential in neuronal repair.[5] They play a critical role in stroke recovery by mediating cell signaling, modulating inflammatory responses, and promoting tissue regeneration.[6–11] Neural stem cell-derived exosomes (NSC-Exo), in particular, have

Received: 11 November 2024
Accepted: 27 January 2025
Published: 21 February 2025

demonstrated significant therapeutic effects, such as inducing angiogenesis, reducing infarct volume, and improving motor function.[12] However, these treatments face challenges, including suboptimal drug loading capacity and rapid clearance from systemic circulation, which limit their efficacy and duration.[13,14] Previous studies have demonstrated that NSC-Exos stimulated by traditional Chinese medicine exhibit a greater capacity for neural repair than exosomes derived from unstimulated cells. This enhanced reparative ability is expected to augment the regenerative potential of the hydrogel we will subsequently develop.[15]

The efficacy of hydrogels as drug delivery vehicles has been increasingly recognized owing to their exceptional biocompatibility, adaptable release characteristics, and substantial capacity for encapsulating therapeutic agents.[16–18] The integration of exosomes with hydrogels offers a promising approach for stroke therapy by enhancing exosome stability and facilitating controlled release kinetics, potentially leading to improved therapeutic outcomes. Given these promising features, addressing the existing limitations of conventional hydrogels, including injectability and passive encapsulation, becomes crucial for advancing their clinical translation. This study aims to overcome these challenges by developing a novel supramolecular hydrogel system.[19,20]

To address these limitations, we developed a novel supramolecular hydrogel system based on active ingredient methylcellulose (HPMC) conjugated with dodecyl isocyanate (HPMC-C12) that was specifically designed to enhance the controlled release of exosomes. The HPMC-C12 hydrogel formed a dynamic network through reversible hydrophobic interactions, which significantly improved exosome retention and prolonged their therapeutic effects in vivo. In comparison with conventional hydrogels, HPMC-C12 demonstrates superior viscoelastic properties, which facilitate more efficient syringe-based administration and make it appropriate for minimally invasive interventions. Furthermore, the dynamic crosslinking mechanism enables precise modulation of exosome release kinetics, ensuring a sustained therapeutic response crucial for chronic neurological conditions such as stroke. By integrating exosomes as active components within the hydrogel matrix, we achieved synergistic interactions that enhanced the therapeutic payload and optimized the delivery profile.[21,22] This innovative hydrogel system represents a significant advancement in exosome-based therapies, offering improved control over the release rate, stability, and targeting specificity.

Materials and Methods

Extraction, Culture and Identification of NSCs

Neural stem cells of primary origin were extracted from the embryonic hippocampus of C57BL/6J mice and maintained in culture using DMEM/F12 medium (Gibco, Carlsbad, CA, USA), supplemented with 2% B27 (Gibco, Grand Island, NY, USA), 20 μg/mL EGF (Sino Biological Inc, Beijing, China), and 20 μg/mL bFGF (Novoprotein Scientific, Suzhou, China). The cells were incubated in a controlled environment with 5% CO2 at 37 °C.

To verify the identity and purity of the cultured cells, we performed immunofluorescence (IF) staining. The neural stem cell (NSC) immunofluorescence (IF) staining protocol involved the initial digestion of NSCs with the Accutase enzyme (Gibco, Grand Island, USA). The resulting centrifuged suspension was deposited onto poly-lysine-coated glass slides and fixed with 4% paraformaldehyde (PFA, w/v, pH 7.4) to facilitate cell adhesion. Permeabilization with Triton X-100 (0.3%) and blocking nonspecific binding sites with goat serum followed.

Afterwards, NSCs were labeled using specific markers, namely SOX2 (1:500, mouse IgG; Abcam, United States) and Nestin (1:500, mouse IgG; Abcam, United States). This labeling was achieved through an overnight incubation with the respective antibodies at 4 °C. After this incubation, the cells were treated with fluorescent secondary antibodies: goat anti-mouse IgG H&L (1:2000, Alexa Fluor 647) and goat anti-mouse IgG H&L (1:2000, Alexa Fluor 488). This treatment occurred at room temperature and lasted for 2 hours.

Nuclei were visualized by staining with 4′,6-diamidino-2-phenylindole (DAPI). The prepared slides were sealed, fixed, and observed using fluorescence microscopy to evaluate the IF staining results.

Isolation and Identification of Exosomes

Neural stem cells underwent three passages in DMEM/F12 medium, and the resulting supernatant was collected. We employed the Buyang Huanwu Decoction to stimulate neural stem cells, as described in previous literature.[15] This

supernatant underwent a series of centrifugation steps: initially filtered through a 0.22μm filter, followed by centrifugation at 2000 g for 10 minutes, then at 10,000 g for 1 hour, and finally ultracentrifuged at 150,000 g for 1.5 hours, all at 4 °C.

The supernatant was discarded following centrifugation, leaving the exosomes at the bottom of the centrifuge tube. These exosomes were resuspended in 80 μL PBS to form a precipitate and then stored in a refrigerator at −80°C.

The Nanoparticle Tracking Analysis (NTA) and Transmission Electron Microscopy (TEM) of Exosomes

The ZetaView system (Particle Metrix, Meerbusch, Germany) was used to assess the distribution of exosome size and number. Exosome samples were diluted tenfold with PBS to achieve an optimal concentration and ensure instrument linearity. Data analysis was conducted using NTA software version 8.05.12 SP2.

For direct observation of exosome morphology, transmission electron microscopy (TEM) was employed (JEOL-1400flash, Tokyo, Japan). To prepare exosome samples for electron microscopy, samples (10 μL) were deposited onto 200-mesh copper grids coated with formvar carbon and incubated for 5 minutes at room temperature. Subsequently, the grids were stained with uranyl acetate following the standard protocol. TEM images were then used to measure the diameter of the exosomes.

Western Blotting (WB) for Exosome Surface Markers

Western blotting (WB) detected specific exosome surface markers, including ALIX, CD9, CD63, TSG101, and Calnexin. Exosomal proteins were extracted using RIPA lysis buffer (Beyotime Biotechnology, Jiangsu, China) and quantified using a BCA kit (Thermofisher, Massachusetts, United States). Proteins from exosomes were isolated using RIPA lysis buffer (Beyotime Biotechnology, Jiangsu, China), and their quantification was conducted using the BCA kit (Thermofisher, Massachusetts, United States). Equal volumes of protein were separated by SDS-PAGE and transferred onto polyvinylidene difluoride membranes.

Subsequently, the membrane was blocked with 5% Bovine Serum Albumin in PBS for one hour at room temperature. Following the blocking step, the membrane was incubated overnight at 4 °C with specific primary antibodies: ALIX (1:1000; Abcam, Cambridge, UK), CD9 (1:2000; Abcam, Cambridge, UK), TSG101 (1:1000; Abcam, Cambridge, UK), and Calnexin (1:1000; Abcam, Cambridge, UK). The membrane was then incubated with horseradish peroxidase-conjugated secondary antibodies at room temperature for two hours. An enhanced chemiluminescence (ECL) assay was performed according to the manufacturer's instructions, and images were acquired using the chemiluminescence method.

Dodecyl-Modified active ingredient methylcellulose (HPMC-C12) Synthesis

HPMC-C12 was prepared according to previously established methods.[23] In summary, 1 g of Dodecyl-modified active ingredient methylcellulose (HPMC, Sigma Aldrich, America) was dissolved in 40 mL of N-methylpyrrolidone (NMP) and heated to 80 °C in a Polyethylene Glycol (PEG) bath while stirring. Dodecyl isocyanate (125 μL, 99%, 125 μL, 0.52 mmol) was diluted in 5 mL of NMP and dropped into the Hypromellose solution. N, N-diisopropylethylamine (10 drops, Macklin, China) was added dropwise, and the mixture was allowed to react overnight with the heat turned off. The resulting polymer was precipitated in a 600 mL bath of acetone and then dissolved in 40 mL of Millipore water. The dissolved polymer was purified through dialysis (3.5 kDa MWCO, Millipore, America) over four days at room temperature. Pure HPMC-C12 was lyophilized and dissolved in 1x sterile PBS to create a 6wt% solution, which was stored at 4°C until use, following the described procedure.

Extrusion and Particle Size Testing of Exosomes

Exosomes were extruded through 100 and 50 nm polycarbonate filters (10 filtrations per membrane) using a pneumatic extrusion unit (GExtruder-100mL, Genizer, America). Exosome size and homogeneity were confirmed by dynamic light scattering measurements using a Zetasizer Lab instrument (Malvern, England).

https://doi.org/10.2147/IJN.S505792

Synthesis of Exo-HPMC Hydrogel

Exo-HPMC hydrogels were prepared by combining the HPMC-C12 stock solution and exosomes stock solution, which were diluted to the desired concentration, using a previously described method. Briefly, 400 mg of HPMC-C12 stock solution was loaded into a 1 mL luer lock syringe. Simultaneously, 600 μL of exosomes stock solution was mixed with 200 μL of PBS and loaded into another 1 mL luer lock syringe. A syringe containing the HPMC-C12 solution was connected to a female luer × female luer elbow fitting. The solution was pushed through the elbow to eliminate air in the connection. Subsequently, an exosome-filled syringe was attached to the other side of the elbow fitting. The solutions were mixed through the elbow at a relatively fast rate for more than 50 cycles, where one cycle constituted the complete transfer of the material from one syringe to another, and then back into the original syringe. This rigorous mixing process was continued until a homogeneous hydrogel was formed, as previously described.

Images of HPMC-C12 and Exo-HPMC Hydrogel by Scanning Electron Microscope

After freeze-drying, both samples were coated with a thin layer of gold using a sputter-coater in a vacuum chamber. Subsequently, the cross-section and surface morphologies of the samples were examined using a field-emission scanning electron microscope (N7000, Hitachi). This microscopy technique allowed for detailed visualization and analysis of the outer surface characteristics of the samples.

Rheological Characterization of Exo-HPMC Hydrogel

The rheological properties of the Exo-HPMC hydrogel were evaluated using a frequency-sweep test ranging from 0.1 to 10 hz at a strain of 1%. Measurements were conducted using a Thermo Scientific HAAKE Mars stress-controlled rheometer with a Peltier stage set at 37 °C. During the test, the rheometer applied controlled stress to the hydrogel and measured its response to oscillatory deformation within a specified frequency range and strain amplitude.

3D Imaging of Laser Scanning Confocal Microscopy

Fluorescently labeled exosomes were mixed to create fluorescently labeled Exo-HPMC hydrogels. Subsequently, the hydrogels were imaged in three dimensions using a confocal microscope (AXIO Vert. A1&Imager A2, Carl Zeiss Microscopy GmbH, Germany) to observe the distribution of exosomes within the gel matrix. Confocal microscopy enables researchers to obtain high-resolution, detailed images of biological samples, providing insights into the spatial arrangement and localization of fluorescently labeled components, such as exosomes, within the hydrogel structure.

Animal Groups and Middle Cerebral Artery Occlusion Model (MCAO)

C57BL/6J male mice (20–22 g) were purchased from the Southern Medical University Animal Center and approved by the Animal Ethics Committee of Southern Medical University (No. SMUL2022148). 60 mice were randomly divided into 4 groups: Sham group (n = 15), PBS group (n = 15), Exo group (n = 15) and Exo-HPMC group (n = 15), respectively. Sham group, in which mice were not treated. The mice of the PBS group were treated with 20 μL PBS covered with drilled holes in the skull (The coordinates: Bregma −0.5 to −0.35 mm; lateral: left 1.8 to 2.2 mm). The mice of the Exo and Exo-HPMC groups were injected at the same point for 20 μL exosomes and Exo-HPMC hydrogel separately. Except for the Sham group, the mice received intraperitoneal injections of BrdU (50 mg/kg) daily.

Before surgery, the mice underwent an 8-hour fasting period and were anesthetized with an intraperitoneal injection of 3% sodium active ingredient (60 mg/kg). Cerebral ischemia was induced through MCAO following a previously described procedure.[24] MCAO involved occluding the left middle carotid artery by inserting a 6 − 0 nylon monofilament suture into the left internal carotid artery. Reperfusion was initiated by suture removal one hour after occlusion. Mice in the Sham group underwent an identical procedure, without suture insertion. Treatments/PBS injections were administered immediately after MCAO. Mice with Longa scores of 2–3 were selected for subsequent experiments. For " in vivo imaging and tracing of exosomes labeled by DiR" experiments, three mice were randomly selected from each group (PBS, Exo, and Exo-HPMC).

Animal Behavior Test

For the behavioral tests, mice underwent daily training sessions for one week before the induction of the MCAO model. The actual tests were performed on days 1, 3, 7, and 14 following the MCAO procedure.

Behavioral Scores of Mice

The Zea Longa 5-point scale was used to assess the model on days 1, 3, 7, and 14.

Footprint Analysis

On the 14th day post-MCAO model induction, gait and motor coordination were evaluated. Red and green dyes were applied to the front and rear paws of the mice, respectively. Each mouse was placed on absorbent paper within a bordered area and encouraged to walk straight. Subsequently, footprints were digitized and a representative image was captured to assess the coordination of the mice.

Catwalk Gait Analysis

The gait parameters of the mice were recorded one day after the surgical operation and continued to be monitored for 14 days. The mice were gently placed on the Catwalk runway and allowed to traverse spontaneously without pausing in response to any stimuli. To be considered a valid trial, The test mice were required to traverse the runway thrice without interruptions, maintaining a roughly consistent speed within 5 seconds. Moreover, the cumulative count of individual steps within the recorded range must be at most six. Walking speed was meticulously recorded during the trials.

Rotarod Walking Test

The rotator was set to start at 10 rpm and accelerate at 40 rpm (at an accelerated speed of 5 rpm). The procedure involved holding the mouse with its tail and placing it on a rotating rod with its back facing the direction of rotation. The mouse was allowed to acclimate for 10 seconds before the acceleration phase began, ensuring that the mouse was facing forward. If the mouse fell before 10 seconds, the time to drop was noted, and the trial was repeated up to three times. The recorded speed was the first drop speed after 10 seconds.

Strength of Front Paws

The experiment allowed the mice to grasp a metal triangle rod with their forelimbs, while their tails were slowly dragged backwards. The maximum grip strength was recorded as the highest value achieved when the mice released their forelimbs. Each mouse underwent this measurement five times, and the average value was calculated for subsequent statistical analysis.

Laser Speckle Imaging System (LSIS)

The Laser Speckle Imaging System (LSIS) was used to quantify the volume of blood perfusion and the diameter of the blood vessels. Initially, an incision was made along the midsagittal line of the cranial apex, and the serosal membrane on the surface of the skull was carefully removed. Local analgesia was ensured by applying two drops of active ingredient hydrochloride. The LSIS settings, encompassing the focal length, false color threshold, and magnification parameters, were fine-tuned to achieve optimal imaging.

Subsequently, optical imaging was performed on the 1st, 3rd, 7th, and 14th days following MCAO induction and treatment. Data on the volume and diameter of cerebral blood flow perfusion and vessels were extracted offline from the captured images. Percentage values representing cerebral ischemia and ischemia/reperfusion (I/R) were calculated based on the fundamental values obtained from the measurements.

In Vivo Imaging & Tracing of Exosomes Labeled by DiR

For in vivo monitoring of the biodistribution of injected exosomes, exosomes were fluorescently labeled with a 4 mg/mL solution of DiR (1,1-dioctadecyl-3,3,3,3-tetramethylindotricarbocyanine iodide; Umibio Group, Shanghai, China). The labeling solution was added to PBS at a 1:200 ratio, and incubated according to the manufacturer's instructions. Excess dye was removed from the labeled exosomes by centrifugation at 10,000 ×g for 30 minutes at 4 °C. After

ultracentrifugation at 100,000 ×g for 1 hour at 4 °C, the labeled exosomes underwent three washes by resuspending the pellet in PBS. Subsequently, the final pellet was resuspended in PBS, and the supernatant was used as the control.

The DiR-labeled exosomes (DiR-exosomes) were combined with HPMC-C12, and the resulting Exo-HPMC hydrogel was labeled with DiR. Following the above-mentioned method, these labeled exosomes and the Exo-HPMC hydrogel were injected into the MCAO model mice. In vivo, images capturing the distribution of DiR-exosomes were taken using the Living Imaging System (IVIS Lumina XRNS III; Perkin Elmer, Germany) on the 1st, 3rd, 7th, and 14th days after mice were anesthetized.

Preparation of Tissue Sections

After 14 days of MCAO and treatment, the mice were anesthetized with a lethal dose of active ingredient (3% maintenance). The thoracic cavity was carefully opened, and an empty needle was inserted into the heart, creating a small gap in the right atrial appendage. Cold saline was infused through the heart until the mice's viscera became colorless, and liquid overflowed from the right atrial appendage, indicating complete blood replacement by saline. Subsequently, a 4% paraformaldehyde (PFA) solution was infused until the limbs and trunks of the mice became stiff.

After the brain was carefully extracted, it was preserved overnight in PFA at 4°C. It was then placed in a 30% sucrose/PBS solution. They proceeded in this manner until the organs reached the bottom of the container. The 6 μm thick tissue sections were sliced from the organs using a freezing microtome (Thermo Fisher Scientific, USA) to detect infarct volume and conduct immunofluorescence analysis. These sections were collected onto poly-D-lysine-coated anti-offset slides and stored at −80 °C for further study.

IF Staining of Tissue Sections

Tissue sections, prepared as described in Preparation of Tissue Sections, were immunostained with the following primary antibodies: anti-CD31 (1:700, rabbit IgG, Abcam, USA), anti-GFAP (1:1000, rabbit IgG, Cell Signal Technology, USA), anti-BrdU (1:500, mouse IgG1, BD Biosciences, USA), and anti-Tuj1 (Neuronal Class IIIβ-Tubulin, 1:200, rabbit IgG, Abcam, USA).

The following day, the tissue sections were treated with secondary antibodies: goat anti-mouse IgG H&L (1:2000, Alexa Fluor 647) and goat anti-rabbit IgG H&L (1:2000, Alexa Fluor 488) for 2 hours at 37 °C. Nuclei were counter-stained with DAPI for 10 minutes. Immunoreactivity was visualized using a fluorescence microscope (AXIO Vert. A1 and Imager A2; Carl Zeiss Microscopy GmbH, Germany).

For quantification purposes, ImageJ software (NIH, Bethesda, MD) was used to randomly select five fields under the microscope, and these views were then compared. The number of double-positively stained cells in each area was counted, and the cell density was determined by averaging the counts from these five fields using Image J software (NIH, Bethesda, MD).

TUNEL Staining

Cell apoptosis was evaluated using the TUNEL (terminal deoxynucleotidyl transferase dUTP nick end labeling) Cell Apoptosis Detection Kit (Servicebio, China). Briefly, tissues were fixed with 4% paraformaldehyde, washed three times with PBS, and immersed in 50 μL Equilibration Buffer. After a 10-minute incubation at room temperature, the samples were subjected to TdT incubation buffer (Servicebio, China) at 37°C for 60 minutes. The tissues were stained with DAPI for 5 minutes to visualize the nuclei.

Three random fields of view were selected using a fluorescence microscope, and three independent observers counted the TUNEL-positive cells. The TUNEL-positive rate (%) was calculated using the following formula: TUNEL-positive cells/total number of cells × 100.

Statistical Analysis

GraphPad Prism 9.0 (GraphPad Software, Inc., La Jolla, CA, USA) was employed for data and image processing and analysis. All values are presented as the mean ± standard deviation (M ± SD). Changes over time and group differences were analyzed using repeated measures, such as analysis of variance with Bonferroni's post hoc correction for multiple

comparisons. Unpaired t-tests and one-way or two-way analysis of variance (ANOVA) were conducted to determine statistical significance in repeated experiments. A p-value < 0.05 was considered statistically significant in all analyses, denoted as *p < 0.05, **p < 0.01, and ***p < 0.001.

Results

Identification of Neural Stem Cells and Derived Exosomes

Neural stem cells (NSCs) can be cultured in specialized media and dispersed into cell suspensions using the Accutase enzyme during passaging. These dispersed cells can then be inoculated onto cell climbing slices that contain polylysine (Figure 1A). Immunofluorescence was employed to observe the expression of Sox2 and Nestin in the cultured cells. The presence of the neural stem cell markers Nestin and Sox2 indicated that the cultured cells were indeed neural stem cells (Figure 1B). Neural stem cell culture supernatants were extracted into exosomes using a previously described method.[25]

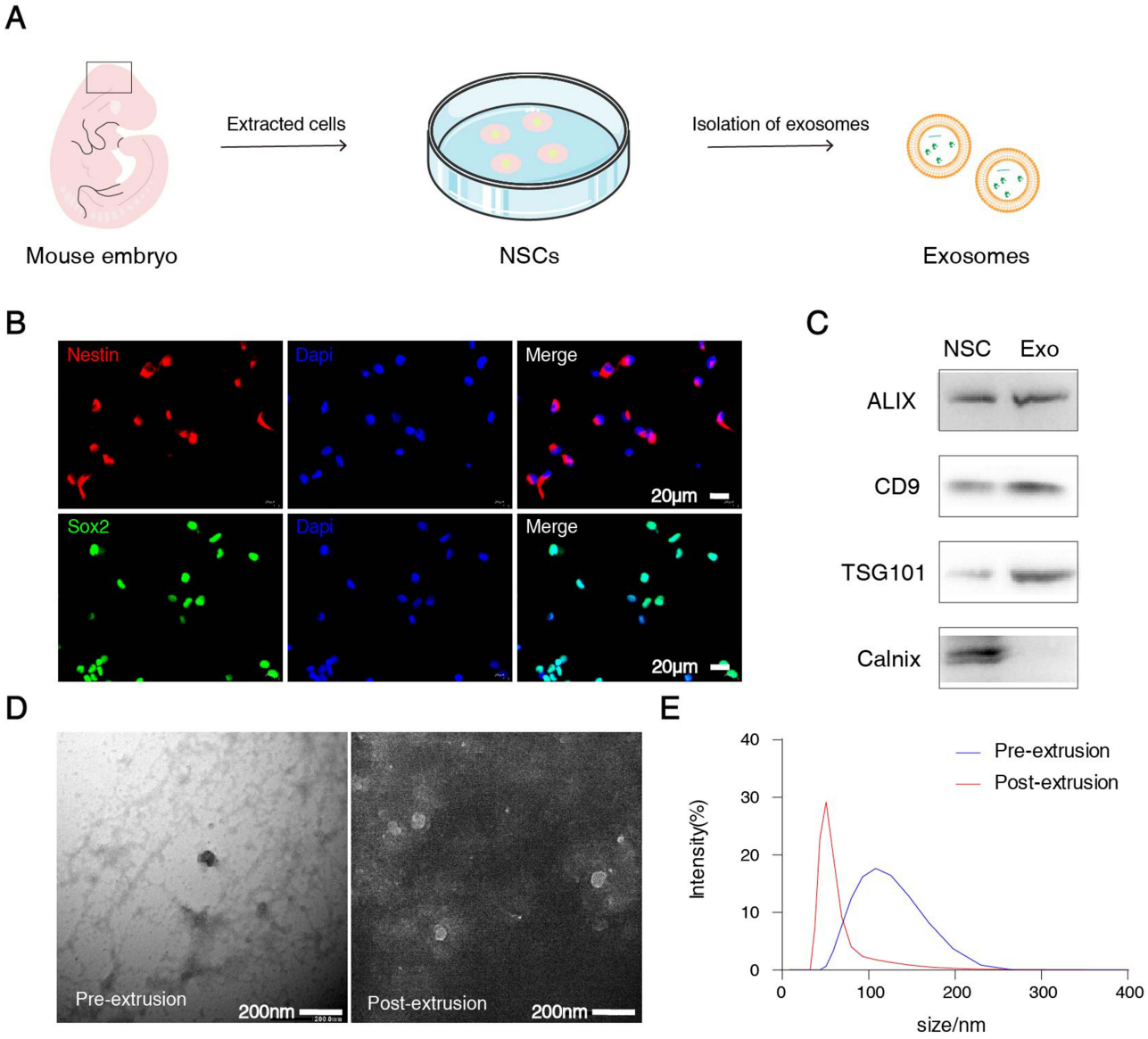

Figure 1 The features of NSCs and exosomes (Exo). (**A**) Immunofluorescence showed the expression of Nestin (red) and Sox2 (green). Nuclei were stained with DAPI (blue). Scale bars: 20 μm in the all panels. (**B**) Western blot analysis of exosomal marker proteins, including Alix, CD9, TSG101 and calnexin (as a negative control). (**C**) The exosome image of NTA analysis. (**D**) NTA analysis shows that the size of exosomes derived from stem cells peaked at 127.5 nm, n=3. (**E**) Particle size distribution of exosomes before and after extrusion.

https://doi.org/10.2147/IJN.S505792

The exosomes obtained were subjected to Western blotting to identify the presence of membrane marker proteins, specifically Alix, CD9, and TSG101. Conversely, Calnexin was not expressed and was used as a negative control (Figure 1C). The Transmission Electron Microscope captured pre- and post-extruded exosomes' images. The resulting photos depict the characteristic structure of the exosomes (Figure 1D). The particle size analysis was conducted using a Malvern particle size analyzer, revealing a discernible disparity in particle size before and after the extrusion process. Following extrusion, more exosomes were observed to have sizes below 100 nm. The peak size was reduced to 60 nm (Figure 1E). The size reduction is considered sufficient for achieving the desired particle size of the assembled hydrogel.[23] Next, we analyzed the images captured by NTA and observed that the particle size distribution (Figure 1E) indicated a peak at 127.5 nm for the exosomes. The results of our analysis suggest that the extracted vesicles were exosomes released by NSCs.

The Characterization of Exosome-Based Supramolecular Hydrogel

The synthesis of the exosome-based supramolecular hydrogel, referred to as Exo-HPMC, was conducted according to a previously reported procedure (Figure 2A).[21,23] Concisely, the compound 1-isocyanatodecane was chemically bonded to HPMC to yield the resulting product known as HPMC-C12, which was subsequently employed in the subsequent stage of the process. Using a pneumatic liposome extruder, the exosomes underwent ten passage cycles through 100 nm and 50 nm polycarbonate filters (Figure 2A). Implementing this procedure reduces the size of exosome particles, consequently augmenting the rigidity of the hydrogel. Mixing plots existed between exosomes and HPMC-C12 with different particle sizes and numbers (S2). The provided image shows the favorable tensile properties of the Exo-HPMC hydrogel (Figure 2B). The rheological properties of the Exo-HPMC hydrogel demonstrated a higher storage modulus (G′) compared to the loss modulus (G″). There was no observed intersection between G′ and G″ within the strain range of 1% to 100% (Figure 2C). The HPMC-C12 and Exo-HPMC hydrogels were subjected to individual freeze-drying processes using a freeze-dryer. Subsequently, the resulting samples were quenched and imaged using a scanning electron microscope (Figure 2D). Visual representations demonstrated that HPMC-C12 exhibited a filamentous morphology characterized by a branching arrangement. Simultaneously, Exo-HPMC displayed a hydrogel-like structure with a significant number of pores resulting from the substantial enrichment of exosomes during the freeze-drying process. The hydrogels were fabricated using the a syringe, which facilitated the formation of hydrogels via rapid extrusion through a three-way valve-like structure (Figure 2E). The Exo-HPMC hydrogel possesses a white hue in its natural state. However, a green pigment was incorporated into the extruded gel to enhance its visual appeal. The injectability of the gel was evident (Figure 2F).

By employing the technique of labeling exosomes with red markers, it was possible to determine the number of exosomes present in each unit of the hydrogel. Furthermore, laser confocal microscopy allowed for the 3D visualization of a substantial distribution of exosomes within the hydrogel (Figure 2G). In summary, the assembly of Exo-HPMC hydrogels was accomplished and the hydrogel properties were characterized.

Sustained Release Effect of Exo-HPMC Hydrogel in Vivo

To quantitatively assess the role of Exo-HPMC in neural regeneration, leachates were collected from the hydrogels on days 1, 3, 7, and 14 and applied to HUVEC cells for 24-hour interventions (Figure 2H). Protein blotting analysis of the samples from each group revealed that short-term exposure to Exo-HPMC leachates had a relatively minor effect on CD31 expression in HUVEC cells. However, prolonged exposure resulted in a gradual increase in CD31 expression, which is indicative of enhanced angiogenesis. This augmentation of vascular endothelial growth is crucial for improving the microenvironment for neural repair, as a robust blood supply is essential for the survival and regeneration of neural tissues.[26–28]

To assess the impact of Exo and Exo-HPMC hydrogels on the prevention of neuroapoptosis, leachates collected on days 1, 3, 7, and 14 were applied to the HT22 cell line for 24 hours (Figure 2I). Caspase3 and BAX were designated as target proteins for our analysis. The results indicated that inhibition of Caspase3 and BAX protein expression in HT22 cells treated with the leachates became more pronounced over time. Notably, the suppression of Caspase3 expression was significant from an early stage, whereas the inhibition of BAX expression intensified over time, ultimately achieving

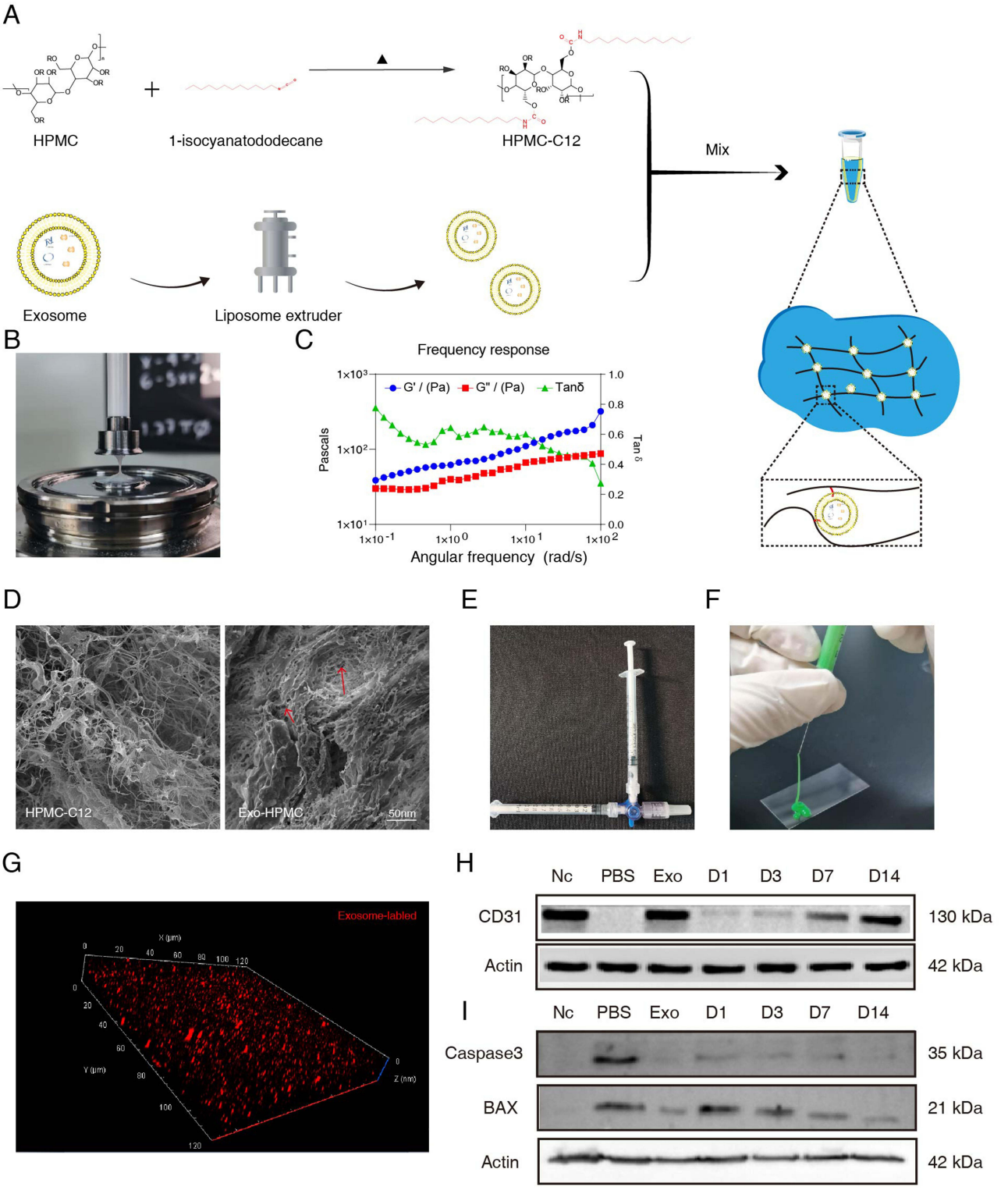

Figure 2 The features and synthesis method of Exo-HPMC hydrogel. (**A**) The synthesis method of Exo-HPMC hydrogel. (**B**) Representative images of the broken filaments of the stretched Exo-HPMC hydrogels. TEM examination of the structure of pre- and post-extruded exosomes. (**C**) Rheological properties of the Exo-HPMC hydrogels. (**D**) Microporous structures of HPMC and Exo-HPMC. (**E**) Mixing methods for preparing supramolecular-based hydrogels and injectability (**F**). (**G**) Three-dimensional image of exosome distribution in the Exo-HPMC hydrogel. Representative Marker protein blotting maps of exosome-based supramolecular hydrogels at different times of leachate intervention in HUVEC cells (**H**) and Ht22 cells (**I**). n = 3/group.

https://doi.org/10.2147/IJN.S505792

protein levels comparable to those in the Exo treatment group by day 14. These findings directly reflect the neuroprotective effects of the hydrogel, suggesting an environment conducive to neuronal survival and regeneration.

DiR, a lipophilic carbocyanine dye with a long-chain structure, is characterized by its prolonged half-life and high fluorescence properties. Hydrogels were prepared by combining DiR-labeled exosomes (DiR-Exos) with HPMC-C12 to facilitate their continuous in vivo release. The role of exosomes in nerve repair was assessed by monitoring the localization and positional changes of the DiR-Exo-HPMC hydrogel post-injection into drilled holes in the cranial vault of mice, specifically targeting the ischemic penumbra. The holes, measuring 1 mm x 1 mm, were created with a cranial drill to accommodate the hydrogel. The coordinates are as follows: Bregma from −0.5 to −0.35 mm, and laterally from 1.8 to 2.2 mm on the left side.

IVIS imaging results demonstrated that in the Exo-HPMC experimental group, the presence of red fluorescent DiR gradually accumulated near the injection site starting at 24 hours post-injection and persisted until day 14 (Figure 3B). In contrast, the DiR-Exo group exhibited a lower red fluorescence intensity than the gel group on day 3, which became nearly imperceptible by day 7 and barely discernible by day 14. These findings suggest that the hydrogel is capable of releasing exosomes in a gradual and sustained manner in vivo, thereby facilitating persistent nerve regeneration within stroke-affected areas.

Exo-HPMC Hydrogel Treatment Improves Neurological Function and Perfusion Volume After Ischemic Stroke

Figure 3A shows a schematic diagram illustrating the animal experimental procedure. The gait analysis was employed to evaluate the coordination of movements after the intervention was administered within 14 days. The examination of behavioral assessments throughout the experiment revealed that mice administered with Exo-HPMC hydrogel injections exhibited enhanced neurological improvement, commencing on day 7 (Figure 3B–E). Based on our estimation, it was hypothesized that during the initial three-day period, the hydrogel group exhibited fewer exosomes than the group receiving a single exosome injection. However, owing to the gradual release characteristic of the hydrogel, its efficacy surpassed that of the other groups by day 7. Significantly, a pronounced visual impact was observed in both grip strength and Rota-rod walking test results (Exo-HPMC vs PBS: $p < 0.001$; Exo-HPMC vs Exo: $p < 0.05$). The Exo-HPMC group exhibited a notable enhancement in motor coordination compared to the other groups (Exo-HPMC vs other groups: $p < 0.05$, Figure 4A). This improvement was particularly evident in behavioral tests such as grip strength and rotarod performance, suggesting significant functional recovery. Interestingly, mice in the Sham group displayed heightened activity, as evidenced by a gait pattern characterized by closely aligned front and hind limb movements, similar to the gait observed in cats. To further quantify recovery patterns, we analyzed the gait velocity of each group. Nevertheless, the remaining groups exhibited tracks of lesser intensity, leading to blurred tracks due to inadequate recovery. Specifically, the tracks of the PBS group showed disorganization and displayed characteristics indicative of a dragging gait.

The catwalk velocity also demonstrated a more pronounced recovery in the Exo-HPMC group than in the other groups (Exo-HPMC vs other groups: $p < 0.05$, as shown in Figure 4C). The laser speckle imaging system (Figure 5A–D) also demonstrated a strong correlation with this phenomenon. The Exo group exhibited marginally superior recovery compared to the gel group on the third day but was subsequently surpassed by the gel group in the subsequent days. Under identical experimental conditions, the Exo-HPMC group exhibited superior recovery on the 14th day compared to the gel group.

Exo-HPMC Hydrogel Promotes Tissue Repair in the Ischemic Model

BrdU/CD31, BrdU/Tuj1, and BrdU/GFAP double-positive cells were quantified within the peri-infarct region after a 14-day treatment period. The immunofluorescence staining revealed a higher abundance of positive cells for both BrdU and Tuj1 near the injury site. The presence of CD31-positive cells was more prevalent and consistent in the hydrogel group than in the other groups (Figure 6A and B). The increase in BrdU/CD31 double-positive cells indicates enhanced angiogenesis in the peri-infarct region, which likely improved perfusion and created a supportive microenvironment for neurogenesis. This phenomenon represents the increased formation of new blood vessels near the lesion. In addition, the proportion of BrdU/GFAP double-

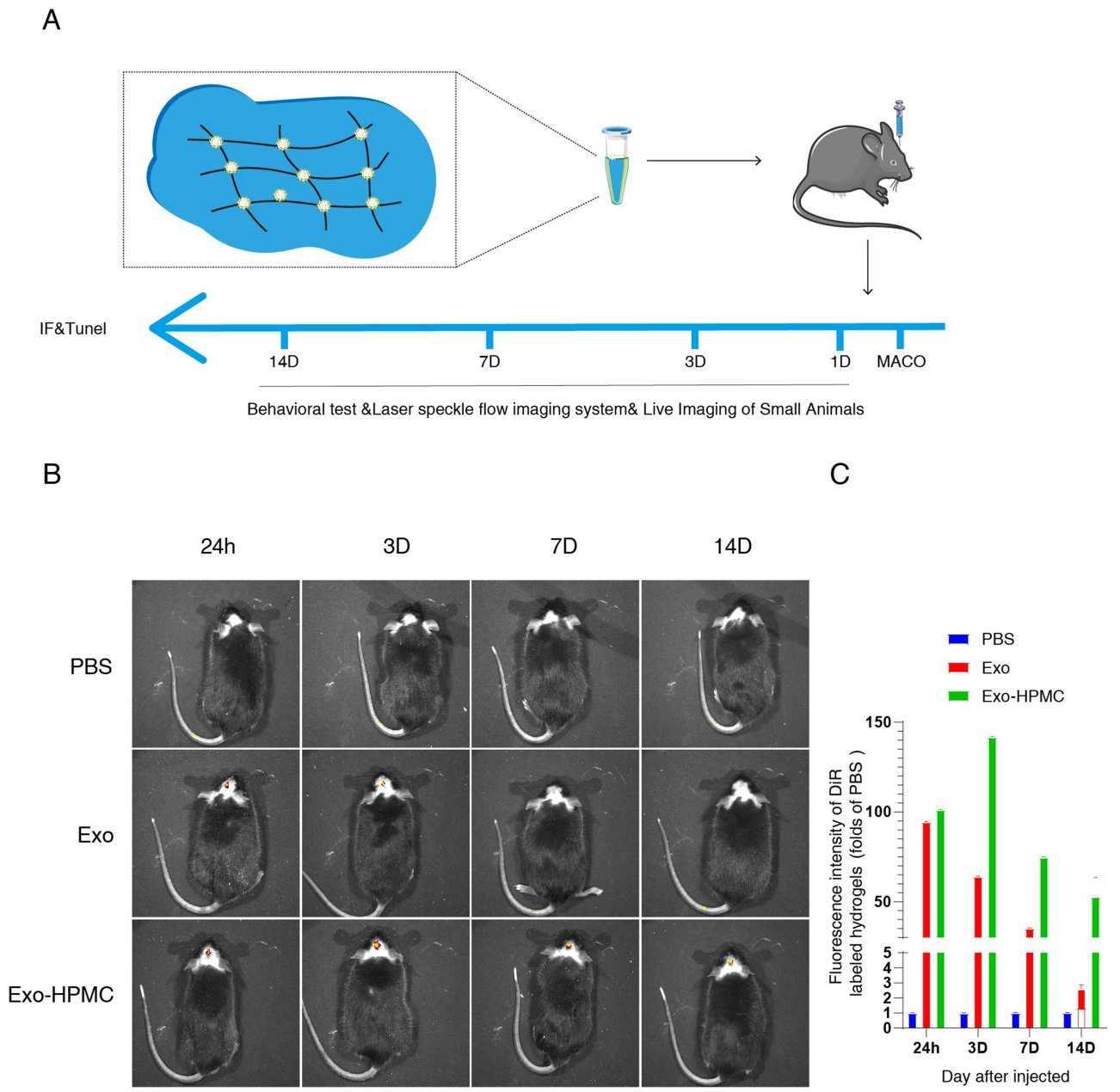

Figure 3 The schematic diagram of overall research and controlled release of Exo-HPMC in vitro. (**A**) The schematic diagram of overall research. (**B**) The distribution of Exo-HPMC (Dir labeled Exo) in injection area in brain tissues. (**C**) Quantification of DiR-labeled hydrogel fluorescence relative to PBS over time. n = 3 for each group.

positive cells in the vicinity of the ischemic region was more significant in the Exo-HPMC group than in the control group (Figure 6C and D). The immunofluorescence staining of cells revealed the presence of newly formed glial cells surrounding the ischemic region. The Exo-HPMC group showed a higher number of BrdU/Tuj1 double-positive cells near the infarct area than the other groups, indicating enhanced production of functional neurons. These results provide a strong foundation for understanding the potential mechanisms underlying Exo-HPMC-induced neurorepair, which will be further discussed in the following section (Figure 6E and F). However, the available evidence does not definitively demonstrate that hydrogels effectively promote nerve repair. Additionally, our findings indicated that the group treated with hydrogels exhibited a lower apoptosis rate (Figure 6G and H).

https://doi.org/10.2147/IJN.S505792

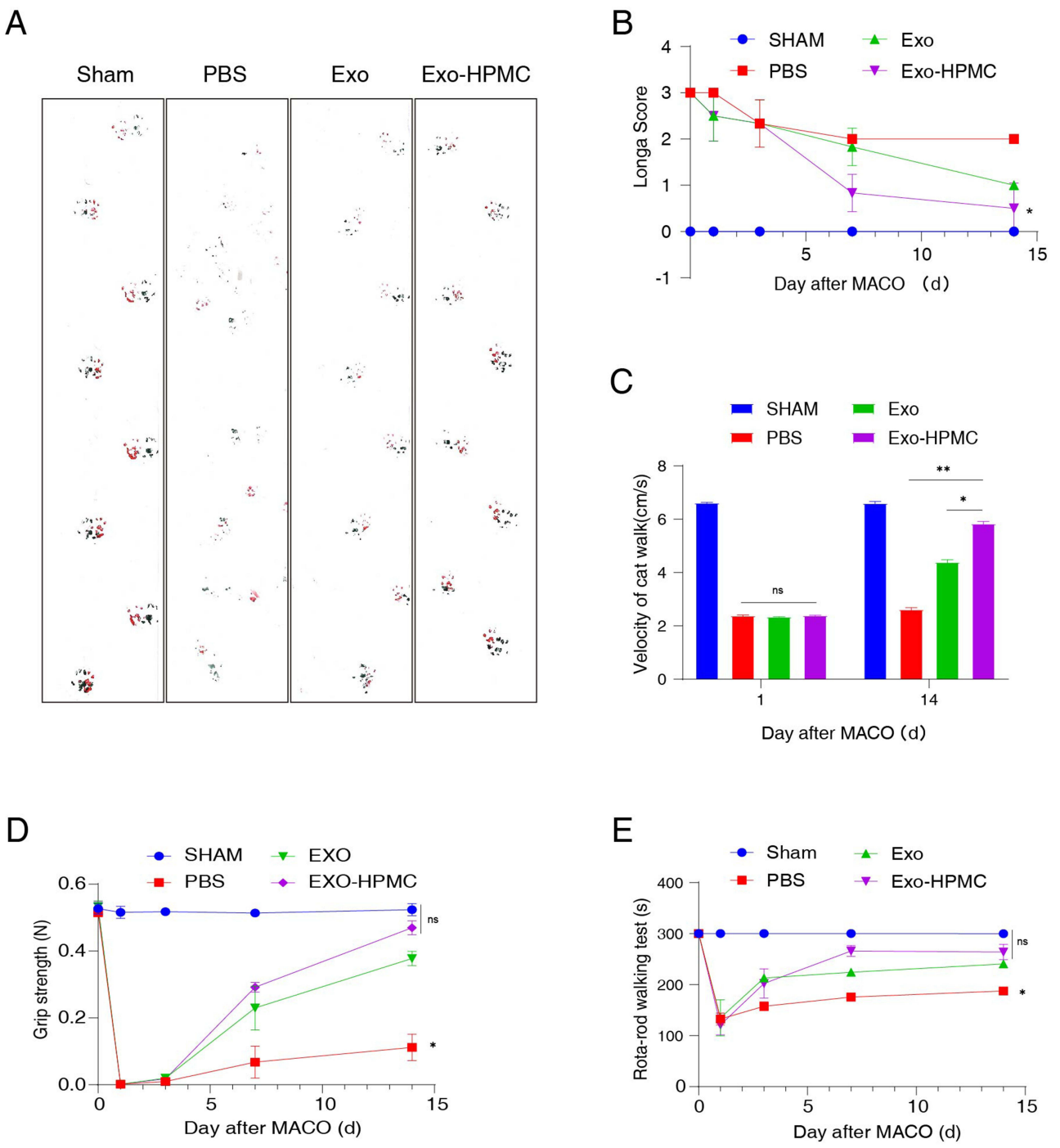

Figure 4 The improvement of neurological function. (**A**) The representative footprints of mice walking 14 days of each group, blue and red footprints represent front paw and hind paw prints, respectively, and unclear footprints represent poor recovery. (**B**) Longa showed neurological improvement in each group. (**C**) The velocity of the catwalk test revealed better behavioral recovery after the treatment of Exo-HPMC hydrogel. n = 6 for each group. (**D**) The grip strength and (**E**) Rota-rod walking test of mice injected by Exo-HPMC was repaired better than of other groups. n = 6 for each group. All data are shown as the mean ± SEM. **P* < 0.05; ***P* < 0.01 (one-way analysis of variance followed by Tukey's post hoc test).

Discussion

Restoring neurological function after ischemic stroke remains a formidable clinical challenge. Over the past decade, neural stem cell (NSC)-derived exosomes have garnered attention for their therapeutic potential due to their ability to cross biological barriers and modulate cellular behavior via bioactive cargo, such as miRNAs and proteins.[24,29–31]

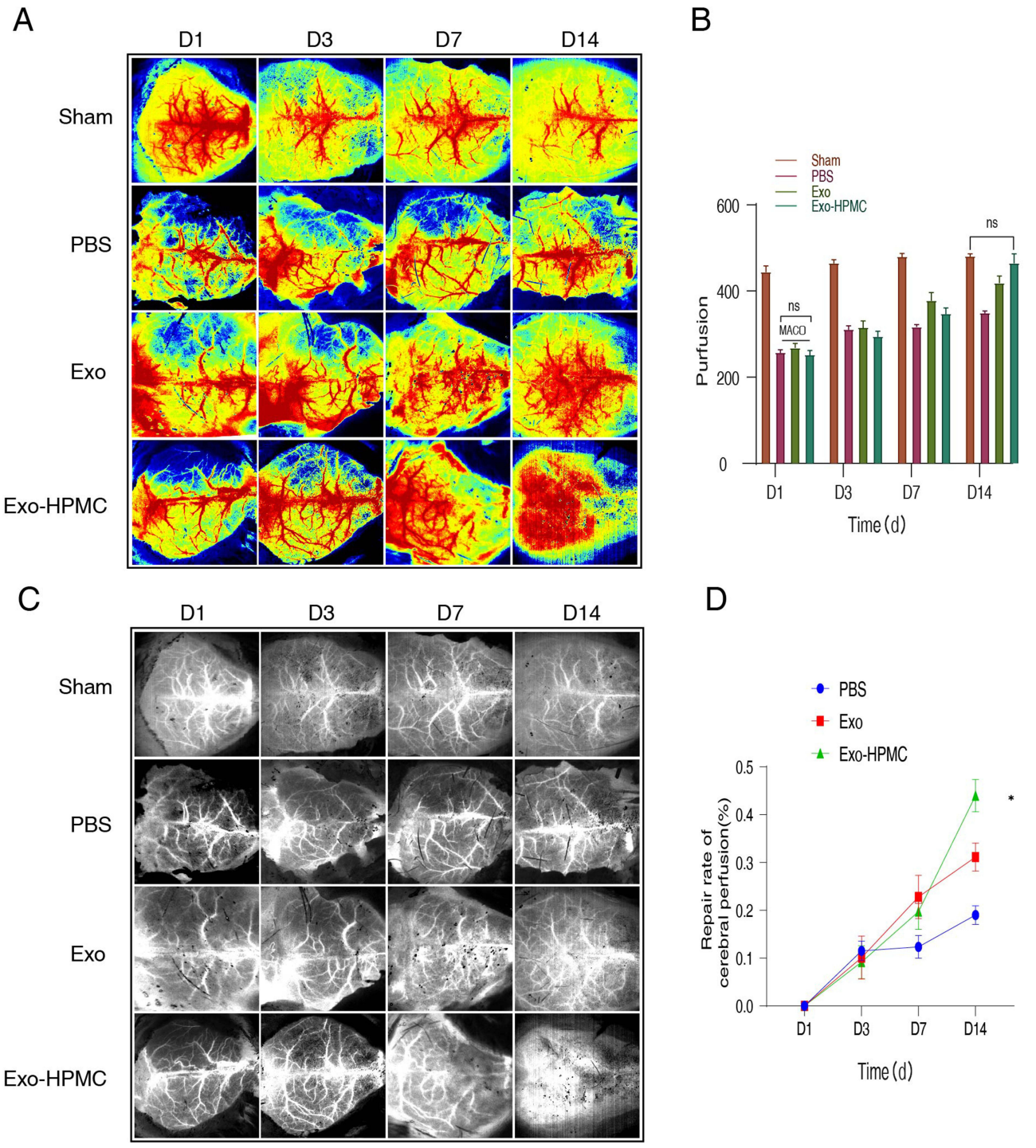

Figure 5 The images and infarct volume by LSIS. The pseudo-colour (**A**) and greyscale (**C**) images of infarct volume following MCAO surgery in each group by LSIS. The quantitative analysis (**B**) and repair rate of left cerebral perfusion (**D**) in each group by LSIS. n = 6 for each group. Ns: no significance, LSIS: Laser speckle imaging system. All data are shown as the mean ± SEM. *$P < 0.05$ (one-way analysis of variance followed by Tukey's post hoc test).

However, rapid clearance and limited therapeutic duration significantly constrain their clinical utility, necessitating innovative strategies to enhance their stability and efficacy.

To address these challenges, we developed an Exo-HPMC hydrogel, which integrates NSC-derived exosomes into an active ingredient methylcellulose (HPMC) scaffold. This hydrogel provides sustained release, prolonging the bioavailability and therapeutic action of exosomes while offering a minimally invasive delivery system with excellent

https://doi.org/10.2147/IJN.S505792

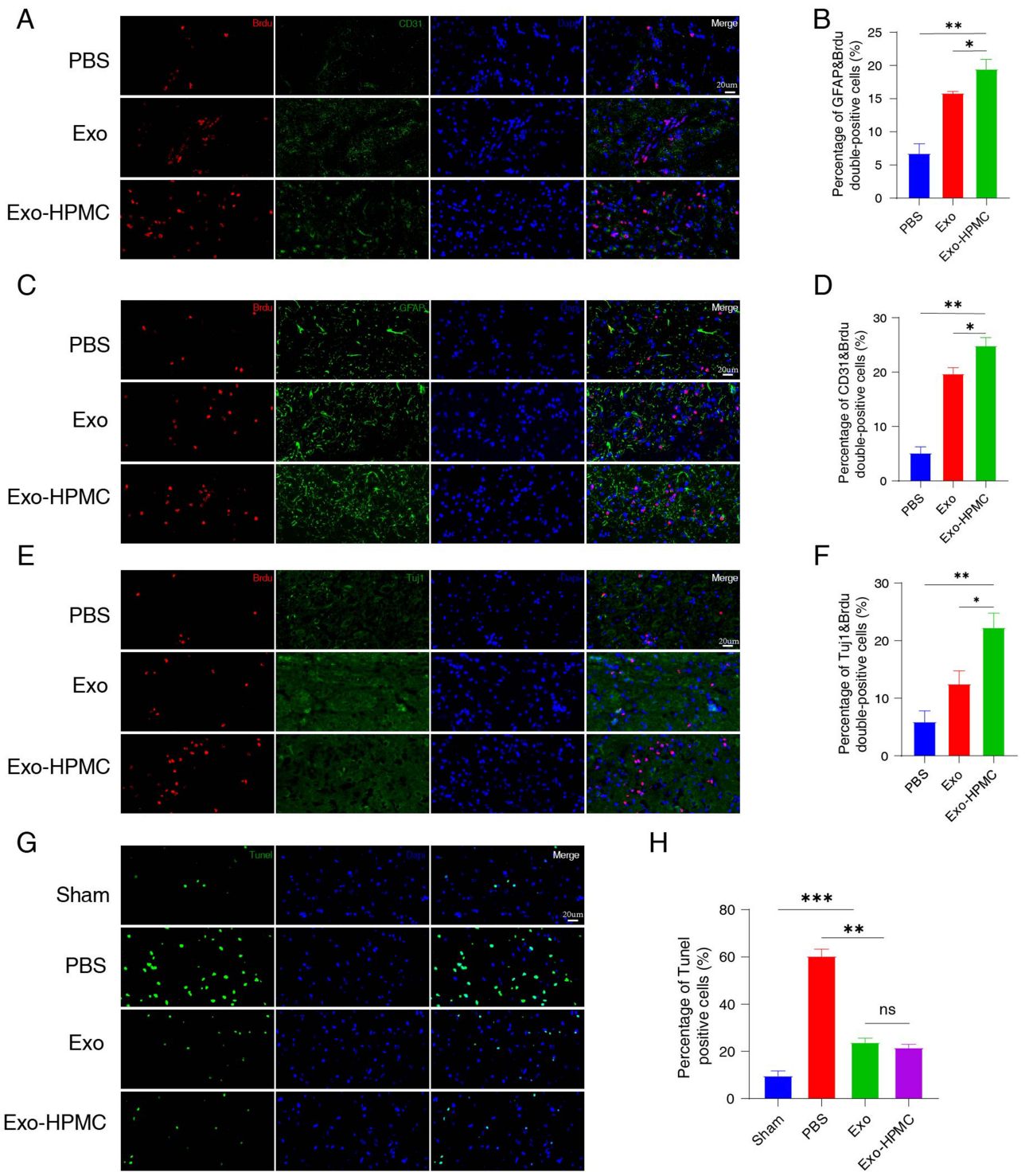

Figure 6 The Exo-HPMC hydrogel promoted in vivo neurogenesis in mice post-stroke. (**A** and **B**) Immunofluorescence double-labeling revealed injection of Exo-HPMC hydrogel into neovascular endothelial cells within the peri-infarct area. Co-localization of BrdU (red) and CD31 (green) was observed. Nuclei were stained with DAPI (blue). Scale bar: 20 μm. n = 6 for each group. (**C** and **D**) Double immunofluorescence staining indicated a higher proportion of BrdU/GFAP double-positive cells in the Exo-HPMC group than in the other groups on day 14 post-treatment. Co-localization of BrdU (red) and GFAP (green) was evident. Nuclei were stained with DAPI (blue). Scale bar: 20 μm. n = 6 for each group. (**E** and **F**) In vivo, double immunofluorescence staining of BrdU and Tuj1 showed an increased number of new neurons in the group injected with Exo-HPMC hydrogel. Co-localization of BrdU (red) and Tuj1 (green) was observed. Nuclei were stained with DAPI (blue). Scale bar: 20 μm. n = 6 for each group. (**G** and **H**) Immunofluorescence demonstrated fewer apoptotic cells (green) in the Exo-HPMC and Exo groups. Nuclei were stained with DAPI (blue). Scale bar: 20 μm. n = 6 for each group. BrdU: bromodeoxyuridine; Exo: exosomes; GFAP: glial fibrillary acidic protein. Data are presented as mean ± SEM. *P < 0.05; **P < 0.01; ***P < 0.001 (one-way analysis of variance followed by Tukey's post hoc test).

injectability and biocompatibility.[32–35] Our findings demonstrated that the Exo-HPMC hydrogel demonstrated superior therapeutic effects, significantly enhancing neuroregeneration and angiogenesis compared to free exosomes in the model of MCAO. These therapeutic benefits can be attributed to the synergistic roles of the hydrogel and the exosomes, which collectively establish a microenvironment conducive to tissue repair.[36,37]

The hydrogel itself stabilizes the exosomes, preventing premature degradation and clearance, while allowing for their controlled release over 14 days. This prolonged availability of bioactive exosomes ensures a continuous modulation of the local microenvironment, supporting cellular repair mechanisms over time. Exosomes are known to mediate key neuroregenerative processes by delivering miRNAs and proteins that modulate angiogenic and neurogenic pathways.[38] For example, exosome cargo such as VEGF and specific miRNAs promote vascular endothelial cell proliferation and migration, facilitating angiogenesis.[39] This vascular remodeling not only improves blood supply to the peri-infarct area but also creates a supportive niche for neuronal repair. In addition, exosome-mediated downregulation of pro-inflammatory cytokines mitigates neuroinflammation, which is critical for fostering an environment favorable for neurogenesis.[40] Our findings further suggest that the interplay between angiogenesis and neurogenesis, as evidenced by increased CD31 and Tuj1 expression (Figure 6A–F), plays a pivotal role in driving the observed functional recovery. Specifically, the increase in BrdU/CD31 double-positive cells indicates enhanced angiogenesis in the peri-infarct region, which likely improved perfusion and created a supportive microenvironment for neurogenesis. This highlights the therapeutic potential of the Exo-HPMC hydrogel in promoting a synergistic repair process. Previous studies have established that enhanced vascularization improves the survival and integration of newly formed neurons, and the Exo-HPMC hydrogel appears to facilitate this crosstalk by promoting consistent blood perfusion, as shown in the laser speckle imaging results (Figure 5A–D).[41,42]

The findings from this study highlight the significant potential of Exo-HPMC hydrogel in promoting neurogenesis, angiogenesis, and functional recovery after ischemic stroke. However, translating these preclinical successes into clinical applications presents several challenges. One of the key considerations is the potential for immune or inflammatory responses triggered by either the hydrogel matrix or the exosomes. While this study demonstrated excellent biocompatibility in mice, it is essential to conduct further evaluations of immunogenicity and inflammatory profiles in preclinical models, particularly given the variability in exosome composition depending on their cellular source and preparation method. Another critical factor is the degradation behavior of the hydrogel under physiological conditions. The in vivo degradation kinetics, influenced by factors such as pH and enzymatic activity, remain uncharacterized in this study. Optimizing the degradation rate is crucial to ensure that the hydrogel provides sustained release of exosomes while avoiding premature collapse or excessive persistence, which could impede tissue remodeling or cause adverse effects.

In addition to safety and stability considerations, scaling up the production of clinical-grade exosomes presents significant technical and regulatory challenges. Standardizing exosome isolation, characterization, and quality control processes will be essential to ensure batch-to-batch consistency and reproducibility, particularly as the field moves toward large-scale clinical applications. Furthermore, testing the hydrogel in larger animal models will be a necessary step to better evaluate its therapeutic potential and address scalability issues in preparation for human trials.

While this study provides strong evidence for the potential of Exo-HPMC hydrogels in stroke recovery, several questions remain unanswered. Future research should also focus on further elucidating the specific mechanisms by which exosomes drive neuroregeneration. While this study provides evidence for the hydrogel's ability to support angiogenesis and neurogenesis, the exact molecular pathways involved remain unclear. Identifying the bioactive components of exosomes responsible for these effects could enable the development of more targeted therapies, potentially enhancing efficacy while reducing variability. Additionally, optimizing the hydrogel's properties, such as crosslink density and mechanical stability, could improve its performance across a range of clinical scenarios.

In summary, the Exo-HPMC hydrogel represents a promising therapeutic platform for ischemic stroke treatment by providing sustained exosome release, promoting neuroregeneration, and improving functional recovery. While this study establishes a strong foundation for its potential application, addressing the outlined challenges related to safety, stability, and scalability will be critical for advancing this technology toward clinical translation.

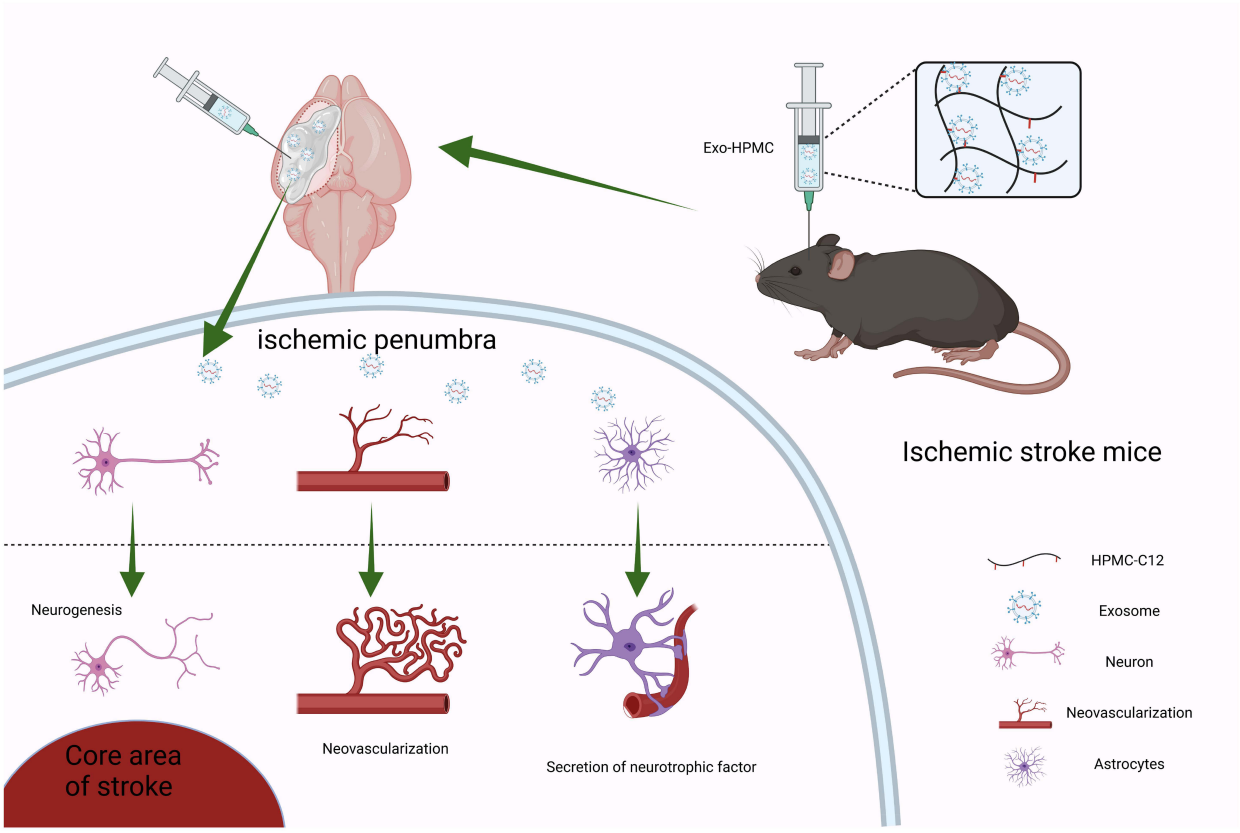

Figure 7 Schematic diagram of exosome-based supramolecular hydrogels for neural repair after ischemic stroke. Created in BioRender. Smith, S (2025) https://BioRender.com/u73b925.

Conclusion

This study highlights the potential of NSC-derived exosome-based hydrogels (Exo-HPMCs) to enhance post-stroke rehabilitation. The Exo-HPMC hydrogel exhibited prolonged exosome release, improved cerebral perfusion, and increased neurogenesis and angiogenesis around the ischemic core. Behavioral and imaging analyses confirmed that Exo-HPMC effectively promoted neurological recovery, indicating that this strategy has significant therapeutic potential for treating ischemic stroke. Future work will focus on optimizing the hydrogel formulation and elucidating the mechanisms underlying exosome-mediated repair to maximize clinical benefits.

Abbreviations

BrdU, 5-Bromodeoxyuridinc; CD31, Platelet endothelial cell adhesion molecule-1; DAPI, 4′, 6-diamidino-2-phenylindole; DiR,1, 1-dioctadecyl-3,3,3,3-tetramethy-lindotricarbocyanine iodide; DMEM, Dulbecco's modified eagle medium; GFAP, glial fibrillary acidic protein; HPMC, Active ingredient Methyl Cellulose; IVIS, Living Imaging System; LSIS, Laser speckle imaging system; MCAO, Middle cerebral artery occlusion; NSCs, Neural stem cells; NTA, Nanoparticle tracking analysis; PEG, Polyethylene Glycol; SOX2, Sex determining region Y-box 2; TEM, Transmission electron microscopy; Tuj1, anti-Tubulin β 3; WB, Western blotting.

Data Sharing Statement

All data generated or analyzed during this study are included in this published article.

Consent for Publication

All authors read the manuscript carefully and gave their consent for publication.

Ethics Approval and Consent to Participate

All experimental procedures strictly adhered to institutional guidelines and received approval from the Laboratory Animal Ethics Committee of Southern Medical University.

Acknowledgments

Figure 7 was created using Biorender.com. We thank Biorender for editing the figure.

Author Contributions

All authors made a significant contribution to the work reported, whether that is in the conception, study design, execution, acquisition of data, analysis and interpretation, or in all these areas; took part in drafting, revising or critically reviewing the article; gave final approval of the version to be published; have agreed on the journal to which the article has been submitted; and agree to be accountable for all aspects of the work.

Funding

This work was funded by the National Key R&D Program of China (2022YFA1104900/2022YFA1104904, 2021YFC2400600/2021YFC2400602, 2022YFC3601900/2022YFC3601902), the Innovation Team Project (2023KCXTD007) and the Special project in key areas of Guangdong Province (2021ZDZX2011).

Disclosure

The authors declare no competing financial interests.

References

1. Donkor ES. Stroke in the 21(st) Century: a Snapshot of the Burden, Epidemiology, and Quality of Life. *Stroke Res Treat*. 2018;2018:3238165. doi:10.1155/2018/3238165
2. Tsao CW, Aday AW, Almarzooq ZI, et al. Heart Disease and Stroke Statistics-2023 Update: a Report From the American Heart Association. *Circulation*. 2023;147(8):e93–e621. doi:10.1161/CIR.0000000000001123
3. Powers WJ, Rabinstein AA, Ackerson T, et al. Guidelines for the Early Management of Patients With Acute Ischemic Stroke: 2019 Update to the 2018 Guidelines for the Early Management of Acute Ischemic Stroke: a Guideline for Healthcare Professionals From the American Heart Association/American Stroke Association. *Stroke*. 2019;50(12):e344–e418. doi:10.1161/STR.0000000000000211
4. Thored P, Wood J, Arvidsson A, Cammenga J, Kokaia Z, Lindvall O. Long-term neuroblast migration along blood vessels in an area with transient angiogenesis and increased vascularization after stroke. *Stroke*. 2007;38(11):3032–3039. doi:10.1161/STROKEAHA.107.488445
5. Zhu ZH, Jia F, Ahmed W, et al. Neural stem cell-derived exosome as a nano-sized carrier for BDNF delivery to a rat model of ischemic stroke. *Neural Regen Res*. 2023;18(2):404–409. doi:10.4103/1673-5374.346466
6. Gao ZS, Zhang CJ, Xia N, et al. Berberine-loaded M2 macrophage-derived exosomes for spinal cord injury therapy. *Acta Biomater*. 2021;126:211–223. doi:10.1016/j.actbio.2021.03.018
7. Feng J, Zhang Y, Zhu Z, Gu C, Waqas A, Chen L. Emerging Exosomes and Exosomal MiRNAs in Spinal Cord Injury. *Front Cell Dev Biol*. 2021;9:703989. doi:10.3389/fcell.2021.703989
8. Zhang ZG, Chopp M. Exosomes in stroke pathogenesis and therapy. *J Clin Invest*. 2016;126(4):1190–1197. doi:10.1172/JCI81133
9. Li Y, Wang J, Chen S, et al. miR-137 boosts the neuroprotective effect of endothelial progenitor cell-derived exosomes in oxyhemoglobin-treated SH-SY5Y cells partially via COX2/PGE2 pathway. *Stem Cell Res Ther*. 2020;11(1):330. doi:10.1186/s13287-020-01836-y
10. Tian T, Zhang HX, He CP, et al. Surface functionalized exosomes as targeted drug delivery vehicles for cerebral ischemia therapy. *Biomaterials*. 2018;150:137–149. doi:10.1016/j.biomaterials.2017.10.012
11. Liu YY, Li Y, Wang L, et al. Mesenchymal stem cell-derived exosomes regulate microglia phenotypes: a promising treatment for acute central nervous system injury. *Neural Regen Res*. 2023;18(8):1657–1665. doi:10.4103/1673-5374.363819
12. Zhong D, Cao Y, Li CJ, et al. Neural stem cell-derived exosomes facilitate spinal cord functional recovery after injury by promoting angiogenesis. *Exp Biol Med (Maywood)*. 2020;245(1):54–65. doi:10.1177/1535370219895491
13. Rao D, Huang D, Sang C, Zhong T, Zhang Z, Tang Z. Advances in Mesenchymal Stem Cell-Derived Exosomes as Drug Delivery Vehicles. *Front Bioeng Biotechnol*. 2021;9:797359. doi:10.3389/fbioe.2021.797359
14. Hazrati A, Malekpour K, Soudi S, Hashemi SM. Mesenchymal stromal/stem cells spheroid culture effect on the therapeutic efficacy of these cells and their exosomes: a new strategy to overcome cell therapy limitations. *Biomed Pharmacother*. 2022;152:113211. doi:10.1016/j.biopha.2022.113211
15. Long J, Gu C, Zhang Q, Liu J. Extracellular vesicles from medicated plasma of Buyang Huanwu decoction-preconditioned neural stem cells accelerate neurological recovery following ischemic stroke. *Front Cell Dev Biol*. 2023;11:1096329. doi:10.3389/fcell.2023.1096329
16. Rezabakhsh A, Sokullu E, Rahbarghazi R. Applications, challenges and prospects of mesenchymal stem cell exosomes in regenerative medicine. *Stem Cell Res Ther*. 2021;12(1):521. doi:10.1186/s13287-021-02596-z
17. Gu C, Li Y, Liu J, et al. Neural stem cell-derived exosomes-loaded adhesive hydrogel controlled-release promotes cerebral angiogenesis and neurological function in ischemic stroke. *Exp Neurol*. 2023;370:114547. doi:10.1016/j.expneurol.2023.114547

18. Tsintou M, Dalamagkas K, Moore TL, et al. The use of hydrogel-delivered extracellular vesicles in recovery of motor function in stroke: a testable experimental hypothesis for clinical translation including behavioral and neuroimaging assessment approaches. *Neural Regen Res*. 2021;16 (4):605–613. doi:10.4103/1673-5374.295269
19. Zhang W, Bao B, Jiang F, et al. Promoting Oral Mucosal Wound Healing with a Hydrogel Adhesive Based on a Phototriggered S-Nitrosylation Coupling Reaction. *Adv Mater*. 2021;33(48):e2105667. doi:10.1002/adma.202105667
20. Zarrintaj P, Khodadadi Yazdi M, Youssefi Azarfam M, et al. Injectable Cell-Laden Hydrogels for Tissue Engineering: recent Advances and Future Opportunities. *Tissue Eng Part A*. 2021;27(11–12):821–843. doi:10.1089/ten.tea.2020.0341
21. Correa S, Grosskopf AK, Klich JH, Hernandez HL, Appel EA. Injectable Liposome-based Supramolecular Hydrogels for the Programmable Release of Multiple Protein Drugs. *Matter*. 2022;5(6):1816–1838. doi:10.1016/j.matt.2022.03.001
22. Wu F, Ren Y, Lv W, et al. Generating dual structurally and functionally skin-mimicking hydrogels by crosslinking cell-membrane compartments. *Nat Commun*. 2024;15(1):802. doi:10.1038/s41467-024-45006-7
23. Grosskopf AK, Roth GA, Smith A, Gale EC, Hernandez HL, Appel EA. Injectable supramolecular polymer-nanoparticle hydrogels enhance human mesenchymal stem cell delivery. *Bioeng Transl Med*. 2020;5(1):e10147. doi:10.1002/btm2.10147
24. Li R, W Duan, T Feng, et al. Lycium barbarum polysaccharide inhibits ischemia-induced autophagy by promoting the biogenesis of neural stem cells-derived extracellular vesicles to enhance the delivery of miR-133a-3p. *Chin Med*. 2023;18:117. doi:10.1186/s13020-023-00831-8
25. Zhang G, Zhu Z, Wang H, et al. Exosomes derived from human neural stem cells stimulated by active ingredient gamma improve therapeutic ability in ischemic stroke model. *J Adv Res*. 2020;24:435–445. doi:10.1016/j.jare.2020.05.017
26. Yang P, Xie X, Fang B, Xie X, Fang B. Extracellular vesicle-loaded hydrogels for tissue repair and regeneration. *Mater Today Bio*. 2023;18:100522. doi:10.1016/j.mtbio.2022.100522
27. Xiao P, Gu J, Xu W, et al. RTN4/Nogo-A-S1PR2 negatively regulates angiogenesis and secondary neural repair through enhancing vascular autophagy in the thalamus after cerebral cortical infarction. *Autophagy*. 2022;18(11):2711–2730. doi:10.1080/15548627.2022.2047344
28. Xu W, Wu Y, Lu H, Zhu Y, Ye J, Yang W. Sustained delivery of vascular endothelial growth factor mediated by bioactive methacrylic anhydride hydrogel accelerates peripheral nerve regeneration after crush injury. *Neural Regen Res*. 2022;17(9):2064–2071. doi:10.4103/1673-5374.335166
29. Kaminska A, Radoszkiewicz K, Rybkowska P, Wedzinska A, Sarnowska A. Interaction of Neural Stem Cells (NSCs) and Mesenchymal Stem Cells (MSCs) as a Promising Approach in Brain Study and Nerve Regeneration. *Cells*. 2022;11(9):1464. doi:10.3390/cells11091464
30. Liu D, Lu G, Shi B, et al. ROS-Scavenging Hydrogels Synergize with Neural Stem Cells to Enhance Spinal Cord Injury Repair via Regulating Microenvironment and Facilitating Nerve Regeneration. *Adv Healthc Mater*. 2023;12(18):e2300123. doi:10.1002/adhm.202300123
31. Shao A, Tu S, Lu J, Zhang J. Crosstalk between stem cell and spinal cord injury: pathophysiology and treatment strategies. *Stem Cell Res Ther*. 2019;10(1):238. doi:10.1186/s13287-019-1357-z
32. Pan P, Svirskis D, Waterhouse G, Wu Z. Active ingredient Methylcellulose Bioadhesive Hydrogels for Topical Application and Sustained Drug Release: the Effect of Polyvinylpyrrolidone on the Physicomechanical Properties of Hydrogel. *Pharmaceutics*. 2023;15(9):2360. doi:10.3390/pharmaceutics15092360
33. Mahmoudian M, Ganji F. active ingredient-loaded HPMC microparticles embedded within injectable thermosensitive chitosan hydrogels. *Prog Biomater*. 2017;6(1–2):49–56. doi:10.1007/s40204-017-0066-x
34. Yu H, Xiao Q, Qi G, et al. A Hydrogen Bonds-Crosslinked Hydrogels With Self-Healing and Adhesive Properties for Hemostatic. *Front Bioeng Biotechnol*. 2022;10:855013. doi:10.3389/fbioe.2022.855013
35. Lyu J, Xie D, Bhatia TN, Leak RK, Hu X, Jiang X. Microglial/Macrophage polarization and function in brain injury and repair after stroke. *CNS Neurosci Ther*. 2021;27(5):515–527. doi:10.1111/cns.13620
36. Jiang Y, Li G, Yang C, Kong F, Yuan Z. Multiresponsive Cellulose Nanocrystal Cross-Linked Copolymer Hydrogels for the Controlled Release of Dyes and Drugs. *Polymers*. 2021;13(8):1219. doi:10.3390/polym13081219
37. Viguier A, Boyer C, Chassenieux C, et al. Interpenetrated Si-HPMC/alginate hydrogels as a potential scaffold for human tissue regeneration. *J Mater Sci Mater Med*. 2016;27(5):99. doi:10.1007/s10856-016-5709-2
38. Gotoh S, Kawabori M, Fujimura M. Intranasal administration of stem cell-derived exosomes for central nervous system diseases. *Neural Regen Res*. 2024;19(6):1249–1255. doi:10.4103/1673-5374.385875
39. Zha Y, Wang J, Wang J, Wang J, Wang J, Wang J. Progenitor cell-derived exosomes endowed with VEGF plasmids enhance osteogenic induction and vascular remodeling in large segmental bone defects. *Theranostics*. 2021;11(1):397–409. doi:10.7150/thno.50741
40. Liu X, Zhang M, Liu H, et al. Bone marrow mesenchymal stem cell-derived exosomes attenuate cerebral ischemia-reperfusion injury-induced neuroinflammation and pyroptosis by modulating microglia M1/M2 phenotypes, Exp. *Neurol*. 2021;341:113700. doi:10.1016/j.expneurol.2021.113700
41. Xiong Y, Lin Z, Bu P, et al. A Whole-Course-Repair System Based on Neurogenesis-Angiogenesis Crosstalk and Macrophage Reprogramming Promotes Diabetic Wound Healing. *Adv Mater*. 2023;35(19):e2212300. doi:10.1002/adma.202212300
42. Hatakeyama M, Ninomiya I, Kanazawa M. Angiogenesis and neuronal remodeling after ischemic stroke. *Neural Regen Res*. 2020;15(1):16–19. doi:10.4103/1673-5374.264442